Gram-scale synthesis of UV–vis light active plasmonic photocatalytic nanocomposite based on TiO₂/Au nanorods for degradation of pollutants in water

A. Truppi[a], F. Petronella[a], T. Placido[a], V. Margiotta[a,b], G. Lasorella[a], L. Giotta[c], C. Giannini[d], T. Sibillano[d], S. Murgolo[e], G. Mascolo[e], A. Agostiano[a,b], M.L. Curri[a,*], R. Comparelli[a,*]

[a] CNR-IPCF, Istituto per i Processi Chimico-Fisici, S.S. Bari, c/o Dip. Chimica Via Orabona 4, 70126, Bari, Italy
[b] Università degli Studi di Bari, Dip. Chimica, Via Orabona 4, 70126, Bari, Italy
[c] Dipartimento di Scienze e Tecnologie Biologiche e Ambientali, Università del Salento, S.P. Lecce-Monteroni, 73100, Lecce, Italy
[d] CNR-IC, Istituto di Cristallografia, Via Amendola 122/O, 70126, Bari, Italy
[e] CNR-IRSA, Istituto di Ricerca Sulle Acque, Via F. De Blasio 5, 70132, Bari, Italy

ARTICLE INFO

ABSTRACT

Semiconductor/metal nanocomposites based on anatase TiO₂ nanoparticles and Au nanorods (TiO₂/AuNRs) were prepared by means of a co-precipitation method and subsequently calcinated at increasing temperature (from 250° to 650 °C) obtaining up to 20 g of catalysts. The structure and the morphology of the obtained nanocomposite material were comprehensively characterized by means of electron microscopy (SEM and TEM) and X-ray diffraction techniques. The photocatalytic performance of the TiO₂/AuNRs nanocomposites was investigated as a function of the calcination temperature in experiment of degradation of water pollutants under both UV and UV–vis irradiation, Photocatalytic experiments under UV irradiation were performed by monitoring spectrophotometrically the decolouration of a target compound (methylene blue, MB) in aqueous solution. UV–vis light irradiation was, instead, used for testing the photocatalytic removal of an antibiotic molecule, Nalidixic acid, by monitoring the degradation process by HPLC-MS analysis. Interestingly, TiO₂/AuNRs calcined at 450 °C was up to 2.5 and 3.2 times faster than TiO₂P25 Evonik, that is a commercially available reference material, in the photocatalytic degradation of the Methylene Blue and the Nalidixic Acid, under UV and visible light, respectively. The same nanocomposite material showed a photocatalytic degradation rate for the two target compounds up to 13 times faster than the bare TiO₂-based catalysts.

The obtained results are explained on the basis of the structure and morphology of the nanocomposites, that could be tuned according to the preparative conditions. The role played by the plasmonic domain in the heterostructured materials, either under UV and UV–vis illumination, is also highlighted and discussed.

The overall results indicate that the high photoactivity of TiO₂/AuNRs in the visible range can be profitably exploited in photocatalytic applications, thanks also to the scalability of the proposed synthetic route, thus ultimately envisaging potential innovative solution for environmental remediation.

1. Introduction

In the quest to solve environmental remediation and solar energy conversion issues, plasmonic heterostructures composed of noble metals in combination with nanostructured semiconductors have been attracting tremendous attention [1,2]. Nanostructured TiO₂ has been generally regarded as benchmark material for photocatalysis based on metal oxide semiconductors and its role in such a relevant area has been substantially studied for decades [3]. Nevertheless, bare TiO2

nanoparticles (NPs) are characterized by a wide band gap that limits its photoabsorption to the UV region (λ < 390 nm), being UV light just a small portion (4%) of the whole solar energy spectrum [4]. Modification of titanium (IV) oxide photocatalyst has often been used to enhance its photocatalytic activity and to extend its absorption wavelength range to the visible region. Many research groups demonstrated the beneficial effect of the integration of a noble metal in TiO₂-based photocatalysts. Such an approach generally involves the dispersion of noble metal NPs (mostly Au and Ag, with sizes in the order of tens to

---

* Corresponding authors.
  E-mail addresses: lucia.curri@ba.ipcf.cnr.it (M.L. Curri), roberto.comparelli@cnr.it (R. Comparelli).

hundreds of nanometers) into semiconductor photocatalysts and aims at enhancing the photoreactivity under UV and/or visible light irradiation [3,5]. Compared with the bare semiconductor, noble metal modified photocatalysts, also known as plasmonic photocatalysts, possess two distinct features: (i) a Schottky junction and (ii) localized surface plasmon resonance (LSPR) tuneable in the Vis-NIR range, both beneficial for the photocatalytic activity [6].

In a Schottky junction charge carriers flow from the semiconductor to the metal creating a spatial charge separation across the semiconductor–metal junction that hinder the recombination of photogenerated electron/hole pairs (e^-/h^+). As a consequence, combination with noble metal NPs is expected to inhibit the electron–hole pair recombination by trapping electrons and to facilitate the transfer of holes on the TiO_2 surface. Subramanian et al. demonstrated that, in the case of Au/TiO_2 NPs, the Fermi level energy shifts toward potential more negative than that of bare TiO_2, that results in an increase of the charge storage efficiency and an enhancement of charge separation, and, overall a higher reducing power of the nanocomposite system. Moreover, the particle size has been found to affect the shift of apparent Fermi level (E_F^*), as the smaller are the Au particles the larger is the shift induced in E_F^* [7]. Interestingly, while the effect of the enhanced charge separation can be observed upon UV irradiation, a significant contribution of the metal NPs to the overall photocatalytic efficiency of composite catalysts, also in the visible region, is expected due to their peculiar optical properties. Their plasmon band, which is tunable in the Vis-NIR region, has been found to enhance the TiO_2 photoactivity under visible light or solar light irradiation [8], demonstrating the potential of such anisotropic metal NPs [2,9]. The surface plasmon resonance (SPR) absorption of metal nanorods (NRs) is featured by two bands, corresponding to the collective oscillations of the free conduction band electrons along the longitudinal and transverse axis of the NRs, respectively. The transverse mode shows a resonance signal around 520 nm, somehow in the same position of the SPR band of spherical particles of similar diameter, while the spectral position of the longitudinal mode is positioned at higher wavelength progressively redshifting in the Vis-NIR range as the aspect ratio (defined as the long to short axis ratio) of NRs increases [10]. These phenomena can be ascribed to the charge accumulation along the rod axis (longitudinal plasma) and along a perpendicular direction (transversal plasma), respectively, being the charge accumulation higher for the latter. As the restoring force is proportional to such charge accumulation, less intense forces and consequently smaller resonance frequencies are required for exciting longitudinal plasmon resonance [11]. The absorption properties of metal nanostructures are extremely sensitive to their size, shape, chemical environment, and mutual distance among metal NPs [12,13]. Owing to their tuneable longitudinal plasmon band and their anisotropic shape, cylindrical Au NRs are among the most studied types of plasmonic NPs. AuNPs are usually preferred over other metals such as Ag or Cu, thanks to their lower tendency to oxidation that ensure the long-term photochemical stability of the resulting photocatalytic material [14].

The present work focuses on the synthesis of TiO_2/Au NRs nanocomposites based on pre-synthesized Au NRs as nucleation substrate for the synthesis of TiO_2 NPs by a simple and easily up-scalable co-precipitation procedure followed by calcination. The resulting nanocomposite showed a peculiar morphology featured by Au nanodomains embedded in a TiO_2 sub-micrometric aggregates composed of anatase NPs that can be prepared in scale up to tens of grams.

The composite nanostructures obtained under different experimental conditions, controlling calcination temperature, were tested to evaluate the effect of the materials structure and morphology on the photocatalytic performance both under UV and visible light. Namely, UV irradiation was used in experiments aiming at decolouration of a model dye, the Methylene Blue (MB), while visible light was irradiated for the photocatalytic degradation of Nalidixic Acid (NA). The photocatalytic performance of the prepared nanocomposites was evaluated as a function of the different calcination temperature and compared with that recorded for the bare TiO_2 prepared under the same experimental conditions, calcinated at the corresponding temperature values in order to investigate the possible effect of the plasmonic domain in the nanocomposites and of the calcination temperature. A commercially available photocatalyst, TiO_2 P25 Evonik, was also used as a reference material.

The prepared visible light active plasmonic nanocomposite photocatalyst, obtained by calcination at 450 °C demonstrated the highest photocatalytic performance under UV and visible light irradiation. A degradation rate 2.5 faster than that found for TiO_2 P25 Evonik and 6.4 times higher than that of the bare TiO_2 calcined at the same temperature of the nanocomposite was obtained for the UV-assisted decolouration of MB. In addition, under visible light irradiation the NA degradation rate assisted by the plasmonic nanocomposite was found 3.2 and 13 times faster than that catalysed by using TiO_2 P25 Evonik and the bare TiO_2 calcined at 650 °C, respectively.

Moreover, the possibility of achieving gram scale amounts of photocatalytic nanocomposite further support the great potential and the accessibility of the synthetic procedure towards their application on a real scale.

2. Experimental section

2.1. Materials

All chemicals were used as received without further purification. Titanylsulfate ($TiOSO_4$, 29% TiO_2, 17% H_2SO_4), ammonium bicarbonate (NH_4HCO_3 99%), sodium borohydride ($NaBH_4$, 99%), L-ascorbic acid (99%), hydrogen tetrachloroaurate(III) trihydrate ($HAuCl_4·3H_2O$,99.9%), silver nitrate ($AgNO_3$, 99.9999%), Methylene Blue (3,7-bis(Dimethylamino)-phenazathionium chloride, MB) and all solvents were purchased from Aldrich Chemical reagent. All solvents used were of analytical grade. TiO_2P25 Evonik (TiO_2 P25) was selected as commercial reference material. Nalidixic Acid, (NA; 1-ethyl-1,4-dihydro-7-methyl-4-oxo-1,8-naphthyridine-3-carboxylic acid) and cetyltrimethylammonium bromide (CTAB) were purchased from Fluka. MilliQ water was employed for preparation of all aqueous solutions.

2.2. Synthesis of TiO_2/Au nanorods

The synthesis of TiO_2/AuNRs was performed by following a general co-precipitation technique. AuNRs samples (aspect ratio 3.5$\pm$ 0.5) were synthesized by using a seed-mediated synthetic route based on a two steps procedure [12]. Firstly, 10 mL of "seed" solution was prepared by mixing CTAB (1 mmol) and $HAuCl_4·3H_2O$ (2.5×10^{-3}mmol) at room temperature. Then, 0.6 mL of ice–cold aqueous solution of $NaBH_4$ (0.01 M) were added under vigorous stirring. In the second step, 500 mL of water dispersed CTAB-stabilized Au NRs (5.6×10^{-10}M) were grown by dropwise addition of an ascorbic acid aqueous solution to a mixture of $AgNO_3$, CTAB and $HAuCl_4·3H_2O$ in water. The resulting solution was kept under stirring until it became colourless, indicative for reduction of Au(III) to Au(I) [15]. At this point, 0.8 mL of "seed" solution were added to the growth solution and the resulting mixture was stirred. After preparation, AuNRs solution was purified from uncoordinated CTAB by means of repeated centrifugation cycles at 7000 rpm for 20 min. The obtained water dispersible Au NRs were then dissolved in the aqueous solution of $TiOSO_4$ (1% w/w compared to TiO_2). Such a solution was hydrolyzed by dropwise addition of NH_4HCO_3 under vigorous stirring, thus promoting formation Ti hydroxide species and their precipitation along with Au NRs in a pink slurry. Such a paste was repeatedly washed by means of subsequent cycles of dispersion in water and centrifugation. The precipitate was dried at 110 °C in oven overnight, grinded and calcined at 250 °C, 450 °C and 650 °C respectively, for 2 h in a muffle. Up to 20 g of TiO_2/Au NRs powder were collected per each synthesis.

2.3. Catalysts characterization

2.3.1. UV–vis absorbance spectroscopy and diffuse reflectance spectroscopy

UV–Vis absorption spectra and diffuse reflectance (DR) spectra were recorded with a UV–Vis–NIR Cary 5 (Varian) spectrophotometer. DR spectra were plotted in Kubelka–Munk (KM) arbitrary unit vs wavelength.

2.3.2. Transmission electron microscopy investigation

Transmission electron microscopy (TEM) analysis was performed by a JEOL JEM-1011 operating at 100 kV. The TEM samples were prepared by drop-casting a catalyst suspension in methanol onto a carbon coated TEM grid and letting the solvent to evaporate.

2.3.3. Scanning electron microscopy investigation

Field emission scanning electron microscopy (FE-SEM) was performed by a Zeiss Sigma microscope operating in the range 0.5–20 kV and equipped with an in-lens secondary electron detector and an INCA Energy Dispersive Spectroscopy (EDS) detector. FE-SEM samples were prepared by casting a few drops of catalyst suspension in ethanol onto a silicon slide. Samples were mounted onto stainless-steel sample holders by using double-sided carbon tape and grounded by silver paste.

2.3.4. X-ray diffraction experiments and simulations

Powder patterns were collected by a Rigaku RINT2500 rotating anode diffractometer (50 KV, 200 mA) equipped with a silicon strip Rigaku D/teX Ultra detector. An asymmetric Johansson Ge(111) crystal is used to select the monochromatic Cu $K\alpha 1$ radiation (l = 1.54056 Å). Measurements are executed in transmission mode, by introducing the sample powder in a Lindemann capillary tube. The XRD patterns were analyzed by using a whole-profile Rietveld-based fitting program (QUANTO) [16]. The phase composition of the samples was determined by fitting the XRD patterns with the crystal structure models of TiO_2anatase (space group I41/amd; cell parameters: a = b = 3.78390 Å and c = 9.51266 Å; $\alpha = \beta = \gamma = 90°$) and TiO_2 rutile (space group p 42/m n m; cell parameters: a = 4.59365 Å; b = 4.59365 Å; c = 2.95874 Å; $\alpha = \gamma = 90°$; $\beta = 107.6°$). Quantitative phase analysis was performed and relative weight percentage was determined with a 5% accuracy.

2.3.5. FTIR spectroscopy

Fourier transform infrared (FTIR) spectroscopy of TiO_2 based samples was carried out at room temperature using a Perkin-Elmer Spectrum One Fourier transform infrared (FTIR) spectrometer equipped with a DTGS (deuterated tryglicine sulfate) detector. The spectra for all experiments was collected with a resolution of $4 \, cm^{-1}$ in the range of $850 \, cm^{-1}$–$4000 \, cm^{-1}$.

2.3.6. Specific surface area

BET (Brunauer-Emmett-Teller) specific surface area was obtained by N_2 adsorption- desorption method on powder samples using a Micromeritics ASAP 2020.

2.3.7. Photocatalysis experiments

The photocatalytic properties of the obtained nanocomposites were tested by measuring the decolouration rate of MB under UV light [17]. Moreover, the nanocomposites were tested under irradiation by visible light were successfully employed for the degradation of NA, a widely diffused antibacterial agent of environmental relevance known to be non-biodegradable [18,19]. A commercially available catalyst (TiO_2 P25 EVONIK) was used as a reference material.

2.3.7.1. Decolouration of methylene blue in aqueous solution with suspended catalysts.
The Au modified photocatalytic nanocomposite powder samples were suspended in an aqueous solution of the dye and the photocatalytic activity compared with pure TiO_2 and the commercially available TiO_2P25. In a typical experiment 1 g/L suspension of TiO_2-based catalysts in MB solution ([MB] = 10^{-5}M) at pH 6 was prepared. The solution was left to stir in the dark for 30 min to reach the absorption-desorption equilibrium. After that, the suspension was irradiated by a UV fluorescent lamp (λ = 254 nm; light flu × 0.2 mW/cm^2 determined by radiometer (Delta Ohm Data Logger 9721). At scheduled time interval, aliquots were collected, purified by centrifugation, and the MB concentration was estimated by absorption spectroscopy.

2.3.7.2. Degradation of nalidixid acid in aqueous solution with suspended catalyst.
In a typical experiment, a defined amount (1 g/L) of nanocomposite was suspended in NA solution ([NA] = 10^{-4} M) at pH 2.5. The desired pH was obtained by adding the proper amount of HCl 0.1 M or NaOH 0.1 M. The solution was left to stir in the dark for 30 min to reach the absorption-desorption equilibrium. After that the suspension was irradiated by a QTH lamp (150 W, 250 nm < λ < 3300 nm) equipped with wide band hot mirror filter (310–760 nm; Fig. S1) in order to achieve a light intensity of 0.22 W/cm^2 ~2 SUN determined by radiometer (Delta Ohm Data Logger 9721). At scheduled time interval, aliquots of NA solution were collected and purified by centrifugation, in order to monitor the NA photocatalytic degradation course by HPLC-MS analysis. The residual concentration was obtained by integrating the area of the chromatographic peak corresponding to the elution of the NA. Briefly, 5 μL sample was injected by an Ultimate 3000 System (Thermo Fisher Scientific) interfaced with a high-resolution mass spectrometer, namely a TripleTOF 5600+ system (AB Sciex). The analysis was recorded in TOF-MS scan type mode, using a duo-spray ion source operated in electrospray (ESI) and positive mode. The MS interface gas conditions were as follows (arbitrary units): curtain gas 35, ion source nebulizer gas 55, ion source turbo gas 55. The source voltages were set as follows: IonSpray voltage 5500 V, source temperature 450 °C, declustering potential 80 V. Injections were performed in duplicate. An Acquity UPLC BEH C18 column 2.1 × 150 mm, 1.7 μm, was used for the chromatographic separation, operating at a flow of 0.200 mL/min with a temperature control set at 40 °C. 5 μL samples were injected and eluted with a binary gradient consisting of water (solvent A) and methanol (solvent B) both containing 0.1% formic acid, as follows: 5% B at the initial point, linearly increased to 100% in 12 min and held for 3 min A 7 min equilibration step at 5% B was used at the end of each run with a total run time per sample of 22 min. As for the data processing, the AB Sciex PeakView 2.2 and MultiQuant 3.0.2 software packages were employed.

3. Results and discussion

In recent years, the possibility to embed AuNRs in a TiO_2 matrix opened up the way to a new class of functional materials. Several methods have been proposed to integrate metal NPs in semiconductor-based nanostructured materials, including chemical and thermal methods, photodeposition, sputtering, core–shell nanostructure fabrication [3]. Herein, we propose a co-precipitation procedure followed by a calcination step, in order to exploit pre-synthesized AuNRs as nucleation substrate for the growth of TiO_2 NPs. Rod shaped Au NPs (Au NRs) have been recognized as unique functional material, thanks to the anisotropic shape, the plasmonic properties under visible light and the high ability to accumulate electrons photogenerated under UV light, that make them ideal candidate to improve the photoactivity of bare TiO_2 [19–21].

3.1. Synthesis of TiO₂/Au nanorods

Briefly, Au-modified based catalysts were prepared by suitable modification of a previously reported approach [22] for the gram-scale synthesis of TiO_2 catalysts involving the hydrolysis of $TiOSO_4$ in presence of NH_4HCO_3.
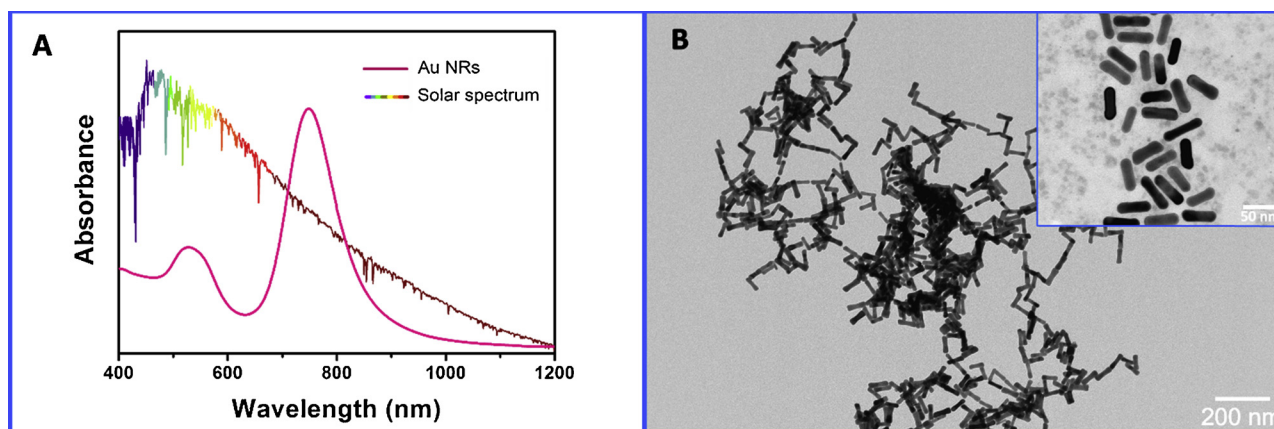
Fig. 1. (A) UV–vis absorption spectra of Au NRs colloidal solution, after purification by centrifugation and re-dispersion in order to remove excess of CTAB compared with solar spectrum at the ground. The spectrum is characterized by the transversal and the longitudinal, plasmon bands, respectively at 530 and 750 nm. Transmission electron microscopy image of the Au NRs. For a statistical determination of the average AuNR size, shape and aspect ratio (AR), at least 200 objects were counted for the sample.

AuNRs with aspect ratio 3.5 ± 0.5 and a longitudinal plasmon band (LPB) centred at 750 nm were prepared and used as nucleation seeds for the growth of TiO_2 NPs (Fig. 1A). Specifically, TEM image (Fig. 1B) indicates that the particle population consists mainly of Au NRs with a 3.5 ± 0.5 AR, with long axis of 55 ± 4 nm and short axis of 15 ± 1 nm.

After the co-precipitation, a deep purple slurry was obtained and dried at 110 °C in oven overnight. TEM micrograph (Fig. S2) shows the presence of dark anisotropic structures in contact with the TiO_2 NPs after a treatment at 110 °C, confirming the presence of AuNRs and the preservation of their anisotropy and the aspect ratio.

Subsequently, the dried paste was calcined in a muffle at three increasing temperature values (250 °C–450 °C–650 °C) in order to investigate the effect of calcination temperature on the crystalline phase of the TiO_2 in the nanocomposite.

TiO_2/AuNRs samples before and after calcination were characterized by SEM and TEM, XRD, BET and DR spectroscopy.

Fig. 2A reports DR spectra of the three TiO_2/AuNRs samples after calcination obtained at the three calcination temperatures.

The spectra of the samples calcined at 250 °C clearly shows the two plasmon bands typical of the AuNRs. In particular, the band corresponding to the transverse mode stays at 520 nm, that is the position recorded for the pristine Au NRs, while the longitudinal plasmon band moves to 900 nm.

The transverse and longitudinal plasmon bands in the spectra of the sample calcined at 450 °C are positioned at 566 nm and 823 nm respectively.

Therefore, the features corresponding to the longitudinal plasmon for the calcined samples at 250° and 450 °C result essentially retained, although shifted towards higher wavelength, consistently with the presence of anisotropic Au NPs.

Interestingly the spectrum of the TiO_2/AuNRs sample calcined at 650 °C shows an evident modification of the line profile of the DR spectrum, being transversal and longitudinal plasmon bands merged in one broad band centred at 624 nm, thus indicating strong modification of NR size and shape [11]. Such an evidence is indicative of a morphological change in the Au NPs, since the appearance of the plasmon band at 624 nm indicate the loss of the anisotropy of the particles, that are, then, likely to have reshaped into rounded NPs [15].

Moreover, the colour of the powder corresponding to the samples treated at the different temperature values, turns from pink to blue by increasing the calcination temperature (Fig. 2B), thus further supporting the change in shape of the Au NPs towards spherical geometry.

SEM micrographs of the TiO_2/AuNRs samples calcined at 250 °C, 450 °C and 650 °C were recorded simultaneously with a secondary

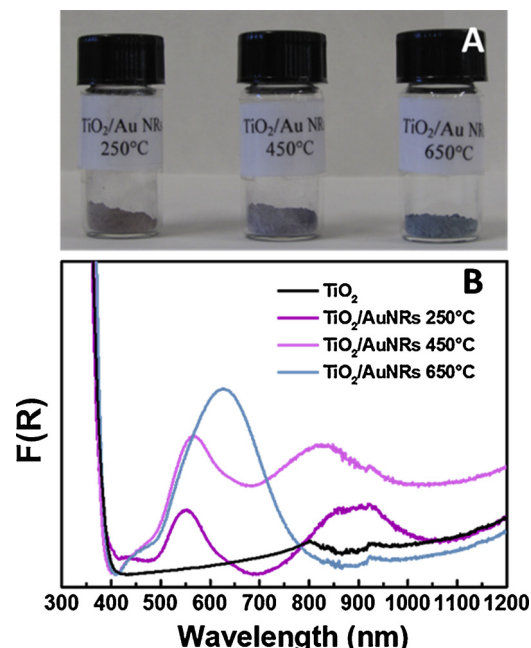**Fig. 2. (A)** Picture of the vials containing the TiO_2/AuNRs nanocatalyst powder samples calcined at three increasing temperatures, 250°, 450° and 650 °C, showing as the colour of the powder changes from deep purple to blue increasing calcination temperature value. **(B)** Diffuse reflectance spectra of TiO_2/Au NRs nanocomposites deposited onto quartz slides, represented as a Kubelka Munk function (F(R)). Reflectance spectra show a blue-shift and a broadening of longitudinal plasmon band absorption as a function of calcination temperature. (For interpretation of the references to colour in this figure legend, the reader is referred to the web version of this article).

electron (SE) and a back scattered electron (BSE) detector, respectively (Fig. 3A–C and A^1– C^1), revealing, for the same area of the sample, information on morphology (SE detector) and chemical composition (BSE detector) [23]. The BSE images in panel A^1, B^1 and C^1 show dark grey areas along with bright anisotropic spots, being such features reasonably ascribed to the TiO_2 nanostructures and to the AuNRs, respectively.

Interestingly, for the sample of TiO_2 NRs/AuNRs treated at 250 °C and at 450 °C, respectively (Fig. $3A^1$, B^1) the bright spots are placed on different focal planes with respect to the surface of the aggregate and hence not visible in the SE topographic micrograph (Fig. 3A, B), which, instead, just accounts for the surface morphology. These results suggest
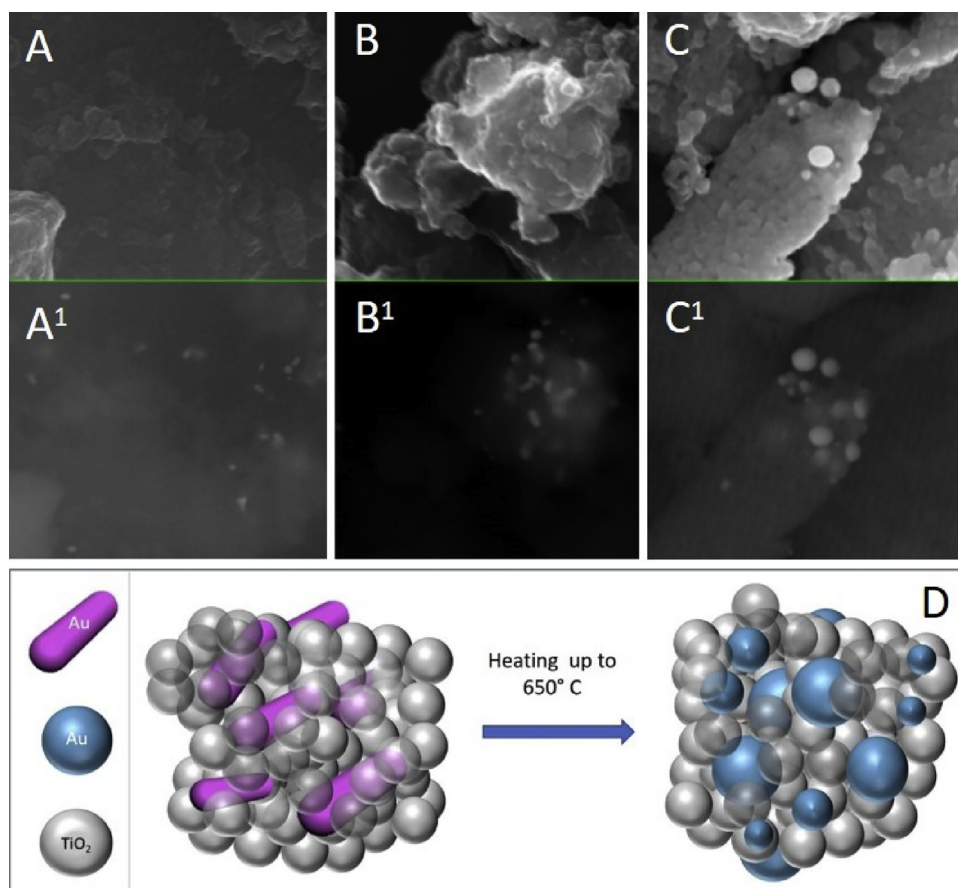
Fig. 3. (A–C) SEM micrographs of TiO$_2$/Au NRs samples calcinated at different temperature values and deposited onto a silicon slide, obtained by in-lens SE detectors (A at 250°, B at 450° and C at 650°) and BSE detector (A^1–C^1). The measurements have been performed with an accelerating voltage of 10–20 kV, a working distance of ~3 mm and an aperture size of 30 μm. (D) Sketch showing the Au NRs, that, while mainly retain their shape and the size upon heating up to 450 °C, undergo reshape leading to spheroidal noble metal structures when thermally treated at 650 °C.

that the AuNRs are embedded within the TiO$_2$ NPs aggregates, that possibly protect them, preventing their reshaping upon calcination. In fact, when the bare "as prepared" AuNRs were treated at the same temperature value a strong modification of the particles and the loss of the anisotropic shape was observed (Fig. S3).

On the contrary, the SEM micrographs of the TiO$_2$/Au sample calcined at 650 °C (Fig. 3C^1) show spherical bright spots both at the surface and inside the TiO$_2$ NPs aggregates. Therefore, the Au NPs can be reasonably assumed to undergo an extensive shape transformation, possibly accompanied to a metal structure migration toward the surface, through the TiO$_2$ NP aggregate structures.

TEM micrographs (Fig. 4) indicate that in the case of the TiO$_2$/AuNRs samples treated at temperature values lower than 650° the presence of NRs can be still detected, whereas in the samples of TiO$_2$/AuNRs treated at 650 °C the anisotropy in the Au NPs seems to be lost leading to nearly spherical NPs, thus confirming the reshape phenomenon suggested by the result of the SEM investigation.

Overall, both TEM and SEM results indicate that Au NPs are mostly embedded in the submicrometric TiO$_2$ NPs aggregates. The morphology of such composite nanostructure can be explained on the basis of the
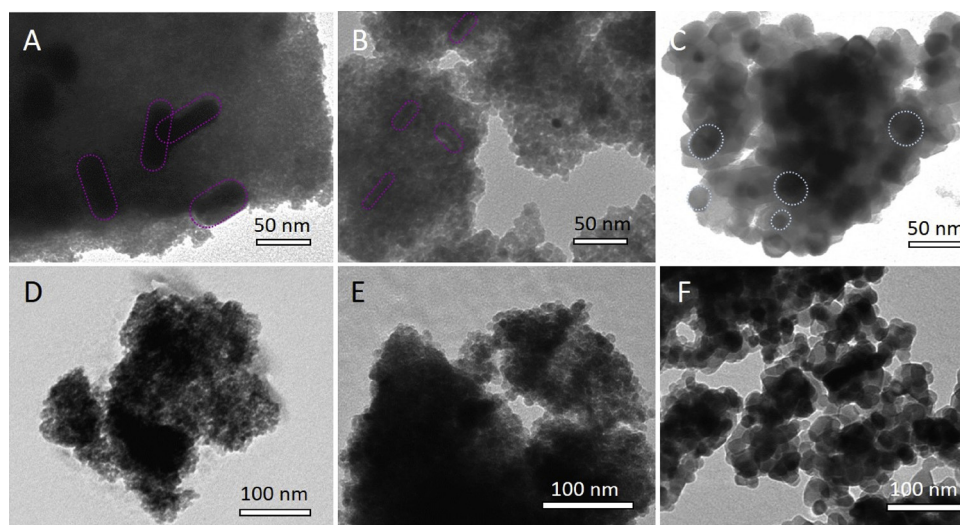

Fig. 4. TEM micrographs of TiO$_2$/AuNRs photocatalysts for different synthetic conditions: TEM micrographs of TiO$_2$/AuNRs 250 °C (A); TiO$_2$/AuNRs 450 °C (B); TiO$_2$/AuNRs 650 °C (C), TiO$_2$ 250 °C (D); TiO$_2$ 450 °C (E) and TiO$_2$ 650 °C (F).
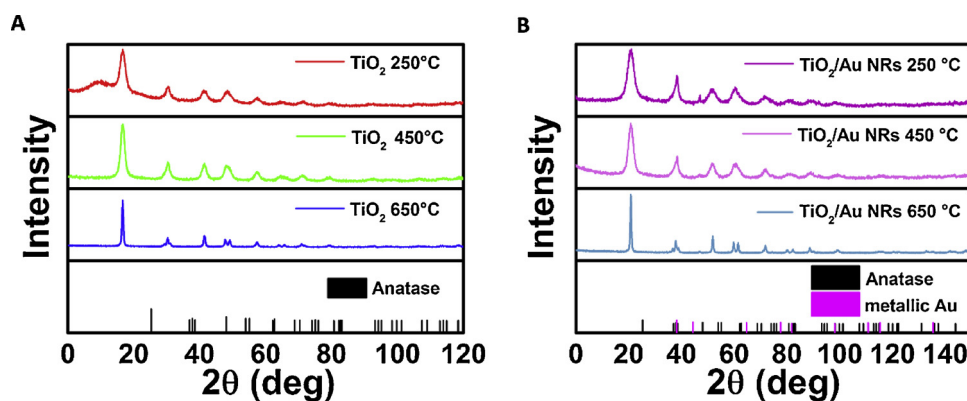
Fig. 5. XRD Diffraction patterns of bare TiO_2 (A) and TiO_2/AuNRs samples (B) at different calcinations temperature: 250 °C, 450 °C and 650 °C. Bragg *hkl* reflections positions for anatase phase (black markers), metallic Au (pink markers).

classical nucleation theory, whereby the activation energy required to grow structures nucleated onto pre-existing particles in a solution, i.e. heterogeneous nucleation, is considerably lower than the barrier for the generation of novel nuclei, i.e. homogeneous nucleation [24]. Therefore the nucleation of TiO_2 NPs in presence of pre-synthetized Au NRs is reasonable to occur as energetically favoured with respect to the formation of novel nuclei in solution, being Au NRs suspended in the reaction mixture able to promote heterogeneous TiO_2 NPs nucleation at their surface and their subsequent growth. Moreover, such a configuration could provide protection of Au nanostructure from the corrosive phenomena [25].

Fig. 5 and Table 1 report the main structural features of both TiO_2 (A) and TiO_2/AuNRs-based photocatalysts (B) as a function of the calcination temperature. Bare TiO_2 samples were found to crystallize in the anatase structure (COD # 7206075, a = b = 3.7852 Å, c = 9.5139 Å, Hermann-Mauguin symmetry space group I 41/a m d) when the calcination temperature value is 250 °C, 450 °C and 650 °C. Analysis of the XRD patterns reveals that the size of the crystalline domain for the TiO_2 NPs increases with temperature values, passing from 5 nm at 250 °C, to 6 nm at 450 °C and finally to 14 nm at 650 °C.

For the TiO_2/AuNRs samples calcinated at the three temperature values, the recorded diffraction patterns can be explained for the three cases, as a mixture of the anatase TiO_2 (COD # 7206075) and Au (COD # 9008463, a = b = c = 4.07825 Å, Hermann-Mauguin symmetry space group F m −3 m) crystal structures. From the XRD data, the weight fractions of anatase and Au, as well as the crystallite size in each sample was calculated. The crystallite size sensibly increases for calcination temperatures higher than 450 °C. Indeed, the TiO_2 crystallite size is smaller than 5 nm when calcination is performed at 250 °C and at 450 °C, whereas it increases up to 25 nm when the TiO_2/AuNRs sample is calcinated at 650 °C.

Therefore, the presence of AuNRs was found essentially not to affect the structural features and the crystallite size of the TiO_2 domains when calcination was performed at 250 °C and 450 °C, while the crystallite size of TiO_2 domains increases in presence of Au NRs when calcination is carried out at 650 °C.

The surface area available in the different photocatalysts samples was determined by means of BET (Brunauer-Emmett-Teller) analysis.

Experimental data revealed that in the case of bare TiO_2 the surface area decreased with the increase of calcination temperature. Indeed, the TiO_2 250 °C, the TiO_2 450 °C and the TiO_2 650 °C resulted in BET surface area values of 169 m^2/g, 69 m^2/g and 43 m^2/g respectively as reported in the Table 2. The decrease of the surface area as well as the concomitant increase of the crystallite size, as a function of the calcination temperature were previously observed and associated with the sintering and growth of TiO_2 crystallite [26,27]. In the case of TiO_2/AuNRs nanocomposites, BET surface areas were found to range from 7 to 95 m^2/g (Table 2) [28].

However, any possible distinct relationship between the synthetic conditions of the samples and the surface area of the resulting structures, though previously reported in literature for similar nanocomposites, could not be identified [28]. In fact, it can be reasonably thought that the BET area values could be here likely controlled by the grinding step rather than by the preparative parameters in the synthesis. In particular, the surface area of the materials may be dominated by the effect of the grinding on the size and morphology of the resulting powder, resulting still macroscopically formed of large assembly of NP aggregate.

Moreover, the area of the samples may be also significantly affected by a possible presence of chemical impurities at the nanomaterial surface, deriving from precursor or solvent additive residuals.

Therefore, for assessing this feature, the samples were investigated by FTIR spectroscopy in order to possibly detect presence of impurities at the surface of the prepared nanomaterials (Fig. S4). All the investigated nanocomposite samples were found to present the same types of spectral bands without any significant difference between the TiO_2 and TiO_2/Au nanostructures. The band at 1630 cm^{-1} can attributed to H−O−H symmetric vibration of water molecules absorbed on the surface of all samples. The broad bands at 3045 cm^{-1}–3400 cm^{-1} in all catalysts can be ascribed to the stretching vibration of OH functional groups. Instead, the absorption bands between 1300 cm^{-1} and

Table 1

Main crystallographic features of TiO_2/AuNRs nanocomposites and TiO_2 calcined at 250 °C, 450 °C and 650 °C, respectively.

Sample	Phase 1 anatase (%)	Phase 2 Au (%)	TiO_2 apparent size (nm)
TiO_2/Au NRs 250 °C	98.8 ± 0.3	1.1 ± 0.3	3.9
TiO_2/AuNRs 450 °C	99.50 ± 0.3	0.5 ± 0.3	4.87
TiO_2/AuNRs 650 °C	99.50 ± 0.3	0.5 ± 0.3	25.76
TiO_2 250 °C	100	–	5.08
TiO_2 450 °C	100	–	5.98
TiO_2 650 °C	100	–	14.81

Table 2

BET specific surface area of the catalysts.

Sample	BET (m^2/g)
TiO_2/AuNRs 250 °C	7.5 ± 0.1
TiO_2/AuNRs 450 °C	95.3 ± 0.5
TiO_2/AuNRs 650 °C	25.8 ± 0.1
TiO_2 250 °C	169 ± 1
TiO_2 450 °C	69.1 ± 0.1
TiO_2 650 °C	43.3 ± 0.3
TiO_2 P25	50 ± 15[a]

[a] Value reported in Technical Information 1243 by Evonik Industries [29].

$1000\,\mathrm{cm}^{-1}$ can be attributed to the sulfate vibration modes, as reported in literature [30–32]. In details, the bands at $1043\,\mathrm{cm}^{-1}$ can be assigned to asymmetric stretching of the S—O bond. The bands at $1211\,\mathrm{cm}^{-1}$ and $1138\,\mathrm{cm}^{-1}$ correspond to asymmetric and symmetric stretches of the S=O bond, respectively. Overall these spectral features can be safely ascribed to residues of the surface anions of the Ti precursor ($TiOSO_4$) that has been used in the synthesis of the samples.

The occurrence of such residual impurities may also account for the unexpected trend observed in the surface area values of the samples, as their uncontrolled and arbitrary adsorption at the powder surface, randomly modifying the surface characteristics of the materials, may be responsible of the deviation from the expected values of the surface area of the samples, as their uncontrolled and arbitrary adsorption at the powder surface may be responsible of the observed deviation from the predictable trend of decreasing surface areas at increasing temperature [33].

3.2. Photocatalysis experiments

3.2.1. Decolouration of methylene blue assisted by the suspended nanocomposite photocatalysts

The photocatalytic activity of the TiO_2/AuNRs powders was preliminarily evaluated performimg a fast screening test of decolouration experiments on a model molecule, namely a dye, the MB (10^{-5}M, pH6) under UV irradiation (Fig. 6), intending to accomplish an initial indication of the overall trend of the catalyst performance. The MB was selected as a target compound extensively investigated in semiconductor photocatalysis, since the photocatalytic performance of the prepared nanocomposites can be assessed by simply monitoring the decolouration of MB in aqueous solution via UV/vis spectrophotometry [17]. Reference tests carried out without photocatalysts and in the dark, respectively, demonstrated that no detectable degradation of MB could be observed under either of these conditions.

Fig. 6 displays the kinetic of MB decolouration, under UV light irradiation by reporting $Ln(C/C_0)$ vs. reaction time, representing, k, the slope of the line plot (Table 3) the apparent rate constant. The ratio between the kinetic constant (k(new catalyst)/ k(reference)) was used a convenient parameter to compare the results of the photocatalytic experiments carried out under the same experimental conditions, including amount of catalyst and pH (Table 3) by using a reference catalyst.

The experimental results reported in Fig. 6 and Table 3, demonstrate the improved photoactivity of TiO_2/AuNRs calcinated at 450 °C compared to TiO_2 P25 and to bare TiO_2 samples under the investigated conditions.
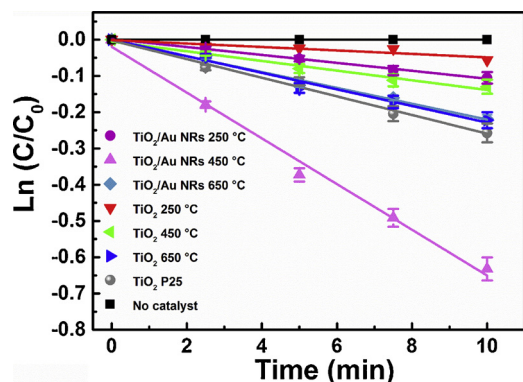

Fig. 6. Comparison of MB decolouration rates in presence of TiO_2/AuNRs 250 °C, TiO_2/AuNRs 650 °C, TiO_2/AuNRs 250 °C, TiO_2 250 °C, TiO_2 450 °C, TiO_2 650 °C and TiO_2 P25. Experiments were carried out at pH 6 under UV light irradiation at 254 nm. MB concentration was been evaluated monitoring the absorbance intensity at 630 nm. The reported data are referred to as mean values ± standard deviation obtained from the analysis of five replicates.

Table 3
Kinetic constants for the MB decolouration process of TiO_2/AuNRs samples nanocomposites in comparison with TiO_2P25 and the corresponding bare TiO_2 calcinated at 250 °C, 450 °C and 650 °C, respectively. Data are reported as the ratio between kinetic constants (k(prepared nanocatalyst) /k(TiO_2 P25)): kinetic constant attained by the investigated catalysts and the kinetic constant attained by TiO_2 P25 (reference).

Sample	$K_{Kinetic}$ (min^{-1}) MB (UV)	$K_{Kinetic\,(new\,materials)}/\,K_{Kinetic\,(TiO2\,P25)}$
TiO_2/AuNRs 250 °C	$(9\pm1)\cdot10^{-3}$	0.3
TiO_2/AuNRs 450 °C	$(64\pm1)\cdot10^{-3}$	2.5
TiO_2/AuNRs 650 °C	$(22\pm1)\cdot10^{-3}$	0.8
TiO_2 250 °C	$(5\pm1)\cdot10^{-3}$	0.2
TiO_2 450 °C	$(10\pm1)\cdot10^{-3}$	0.4
TiO_2 650 °C	$(23\pm1)\cdot10^{-3}$	0.9
TiO_2 P25	$(26\pm1)\cdot10^{-3}$	1
No catalyst	0	–

For the TiO_2 and TiO_2/AuNRs calcinated at 250 °C (TiO_2/AuNRs 250 °C) the kinetic constant was found 5 10^{-3} min^{-1} and 9 10^{-3} min^{-1}, respectively. When the calcination temperature rises at 450 °C for the TiO_2/AuNRs the kinetic constant was found 6.4 times higher than that for the bare TiO_2 calcined at the same temperature value. Finally, the TiO_2 and TiO_2/AuNRs treated at 650 °C (TiO_2/AuNRs 650 °C) reported comparable kinetic constants. Therefore, the presence of AuNRs in the nanocomposites turned in an increase of the photocatalytic performance, particularly evident for the TiO_2/AuNRs calcinated at 450 °C (TiO_2/AuNRs 450 °C). Indeed, based on the kinetic constants, the rate of the reaction assisted by TiO_2/AuNRs 450 °C is found 2.9 time higher than that catalysed by TiO_2/AuNRs 650 °C, and 7 time higher than that carried out in presence of TiO_2/AuNRs 250 °C. Remarkably, the TiO_2/AuNRs 450 °C demonstrated a 2.5 higher photocatalytic activity also with respect to the commercially available photocatalyst, namely TiO_2 P25 that, in fact, presents a kinetic constant of $26\cdot10^{-3}$ min^{-1}.

In summary, the ability of investigated nanomaterials on the photocatalytic decolouration of MB could be resumed as follows: TiO_2/ AuNRs 450 °C > > TiO_2P25 > TiO_2/AuNRs 650 °C ≅ TiO_2 650 °C > TiO_2 450 °C > TiO_2/AuNRs 250 °C.

The improved photocatalytic activity in the UV region cannot be ascribed just to the increased specific surface area, taking into account the BET area values (Table 2).

In fact, in Fig. S5 the kinetic constant was plotted as function of specific surface area (k = f (surface area)) and no linearity among the kinetic constant and surface area was observed by varying the chemical composition of the TiO_2 based materials.

In fact, although the surface area of the TiO_2/AuNRs calcinated at 450 °C (95.3 ± 0.5 m^2/g) is much lower than that recorded for TiO_2 250 °C sample (169 ± 1 m^2/g), its photoactivity is found 13 times higher, considering the respective apparent kinetic constants. Also, the kinetic constant obtained for TiO_2/AuNRs 250 °C (7.5 ± 0.1 m2/g) is 2 times higher than that achieved by using TiO_2 250 °C (169 ± 1 m2/g), despite its BET area is 22 times lower. These results indicate that the enhancement in the photocatalytic activity should arise from the beneficial effect of the coupling of metal and semiconductor.

It is well established that noble metals in contact with semiconductor particles improve the photocatalytic activity of the resulting nanocomposite, due to the electron transfer processes at the metal/ semiconductor interface. Photogenerated electrons flow from the CB of TiO_2 to the metal (namely from the domain at a higher Fermi level value to the domain with a lower one) to align the Fermi energy levels. This phenomenon results in the formation of a Schottky barrier, with an excess of negative charges on the metal and an excess positive charge on the semiconductor. In between, at the interface of the two components, a depletion layer maintains charge separation, thus hindering the detrimental e$^-$/h$^+$ recombination events [19,20,34].

Indeed, upon TiO_2 photoexcitation promoted by UV light irradiation, photogenerated electrons can flow from the conduction band of TiO_2 to Au NRs where they can accumulate until achieving the Fermi Level equilibration thus remarkably limiting e^-/h^+ pair recombination events and increasing the photocatalytic performances.

The TiO_2/AuNRs 450 °C demonstrated to be the most photoactive among the investigated nanocomposite samples, under the described experimental conditions. Its superior photocatalytic activity, and the highest kinetic constant, can be rationalized on the basis of morphological consideration, e.g. its surface area was reported to be the highest among those of the three TiO_2/AuNRs nanocomposite samples, as reported in the Table 2. Moreover, the enhanced performance of the TiO_2/AuNRs 450 °C with respect to that of the counterpart calcinated at 650 °C could be reasonably ascribed to the shape of Au NPs, that moves from a rod-like geometry in the former, to a spheroidal one in the latter, that could detrimentally affect the electron transfer.

In details, based on geometrical consideration, rod shaped Au NPs, in comparison with spheroidal AuNPs, should provide a higher amount of sites where TiO_2 domains can establish a close interaction with Au surfaces leading to an improvement of TiO_2 CB electron transfer between the semiconductor and the metal.

Moreover, despite the fact that AuNPs preserved their anisotropy also in the TiO_2/AuNRs 250 °C, a reduced photocatalytic activity is exhibited with respect to the TiO_2/AuNRs 450 °C. Such a difference can be reasonably connected to the higher value of specific surface area measured for the TiO_2/AuNRs 450 °C. However, a careful comparison of Fig. 3A1 and B1 shows that TiO_2/AuNRs 450 °C present Au NPs embedded within the TiO_2 matrix, in a densely-packed configuration, that is expected to enhance the close contact between the metal and the semiconductor and therefore to an improved electron transfer.

3.2.2. Degradation of nalidixic acid assisted by the suspended nanocomposite photocatalysts

The photocatalytic activity of the three investigated nanocatalysts, TiO_2/AuNRs calcinated at 250 °C, 450 °C and 650 °C respectively, compared to the bare TiO_2 calcined at the same temperature values and TiO_2 P25 respectively, was investigated in the degradation of NA in aqueous solution. In particular it was employed an aqueous solution ([NA] = 10^{-4} M) at pH 2.5 under visible irradiation by a QTH lamp (0.22 W/cm^2 $\sim$ 2 SUN) for 15 min (Fig. 7). The NA, a fluoroquinolone-based compound, extensively detected in surface water and wastewater, is a suitable model target molecule, being a non-biodegradable
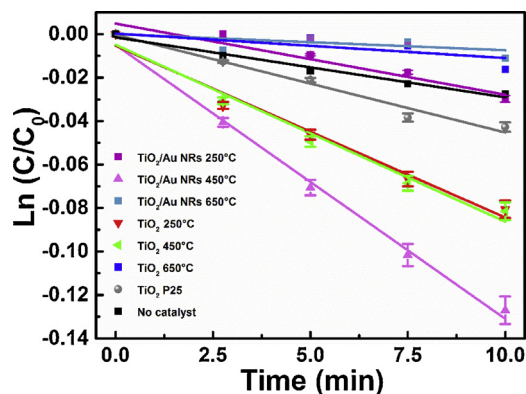

Fig. 7. Time course evolution of NA degradations as function of time in the case of TiO_2/AuNRs 250 °C, TiO_2/AuNRs 450 °C, TiO_2/AuNRs 650 °C, TiO_2 450 °C, TiO_2 450 °C, TiO_2 650 °C and TiO_2 P25 assisted experiments. Experiments were carried out at pH 2.5, in water with suspended catalysts, under visible irradiation by a QTH lamp (150 W, 430 nm < λ < 3300 nm, 0.22 W/cm^2 $\sim$ 2 SUN) equipped with wide band hot mirror filter (400–700 nm). The reaction kinetic was monitored by HPLC-MS analysis. The reported data are referred to as mean values ± standard deviation obtained from the analysis of five replicates.

Table 4
Summary of kinetic constants calculated for the photocatalytic degradation of NA: TiO_2/Au NRs nanocomposites in comparison with TiO_2 P25 and the corresponding bare TiO_2 calcinated at 250 °C, 450 °C and 650 °C, respectively. Data are reported as the ratio between kinetic constants (k(new materials) /k(TiO_2 P25)), a convenient parameter to compare photocatalytic performances in the different samples.

Sample	$K_{Kinetic}$ (min^{-1}) NA (HPLC)	$K_{Kinetic\ (new\ materials)}$/ $K_{Kinetic\ (TiO2\ P25)}$
TiO_2/AuNRs 250 °C	$(3 \pm 1) \cdot 10^{-3}$	0.8
TiO_2/AuNRs 450 °C	$(13 \pm 1) \cdot 10^{-3}$	3.2
TiO_2/AuNRs 650 °C	$(1 \pm 1) \cdot 10^{-3}$	0.3
TiO_2 250 °C	$(8 \pm 1) \cdot 10^{-3}$	2
TiO_2 450 °C	$(8 \pm 1) \cdot 10^{-3}$	2
TiO_2 650 °C	$(1 \pm 1) \cdot 10^{-3}$	0.3
TiO_2 P25	$(4 \pm 1) \cdot 10^{-3}$	1
No catalyst	$(3 \pm 1) \cdot 10^{-3}$	–

antibacterial agent of environmental relevance [19]. Moreover, since NA does not absorb in the visible region, any possible sensitization effect can be safely ruled out.

The reaction course was monitored by HPLC-MS analysis and the kinetic constant, calculated from the area of NA chromatographic peak, reported such as Ln(C/C$_0$) vs irradiation time (Fig. 7). Control experiments performed in absence of any photocatalyst or without irradiation revealed a negligible degradation extent.

The comparison among the apparent kinetic constants shows that the degradation of NA is faster when assisted by TiO_2/AuNRs 450 °C, with respect to the reaction assisted by the other TiO_2/Au NRs samples, the bare TiO_2 samples, irrespectively of the calcination temperature, and TiO_2 P25. Table 4 reports the NA degradation rate of the reaction assisted by the different nanocatalysts, under visible light, as the ratio between the kinetic constant (k(new catalyst)/ k(reference)), which is a suitable parameter to be effectively used to compare their photocatalytic activity. In addition, the degradation percentage of NA was reported for all obtained catalysts after 30 min of irradiation in Table S1.

Interestingly, TiO_2/AuNRs 450 °C demonstrated to be the best performing photocatalytic nanomaterial under visible irradiation promoting a 30% degradation of NA.

Indeed, it exhibited a kinetic higher constant (k = $13 \cdot 10^{-3}$ min^{-1}) in comparison with TiO_2/AuNRs 250 °C and TiO_2/AuNRs 650 °C that conversely showed a kinetic constant of $3 \cdot 10^{-3}$ min^{-1} and $1 \cdot 10^{-3}$ min^{-1} respectively.

The reaction rate catalysed by TiO_2/AuNRs 450 °C is 4 times faster than the photodegradation assisted by the TiO_2/AuNRs 250 °C and more than 10 time faster respect the reaction assisted by the TiO_2/AuNRs 650 °C. Remarkably, the kinetic constant obtained for TiO_2/AuNRs 450 °C is 3.2 times higher than that achieved by using TiO_2P25. Finally, the TiO_2/AuNRs 450 °C is 1.6 time faster than TiO_2 250 °C and TiO_2 450 °C, respectively, under the investigated conditions (Table 2).

However, the slight photoactivity of the TiO_2 250 °C and TiO_2 450 °C catalysts can be due to a possible absorption of UV light despite of a hot mirror filter was used to cut the emission of the lamp. In fact, this filter blocks a very wide band in the infrared region while maintaining good transmittance in the visible range and a weak transmittance in the UV range (Fig. S1).

In summary, the ability of investigated nanomaterials to degrade NA under visible irradiation could be resumed as follows: TiO_2/AuNRs 450 °C > TiO_2 450 °C = TiO_2 250 °C > TiO_2P25.

Also in this case, the enhanced photochemical reactivity of TiO_2/AuNRs nanocomposite under visible light irradiation could be ascribed to the noble metal/semiconductor coupling rather than to the contribution of the specific surface area. In particular, synergistic effects due to the plasmonic properties of the Au NRs, that give rise to an

intense and highly localized electromagnetic field [6,8] much higher in the anisotropic nanostructures, can take place [35]. The plasmonic features of Au NRs can be responsible of two possible photoactivation mechanisms due to (i) hot electron effect and (ii) near field effect [21]. Under LSPR conditions, the generation of the so-called "hot electrons" can be induced by the non-radiative relaxation of the surface plasmons, transferring the accumulated energy to electrons in the conduction band of the metal NPs. Therefore, when the semiconductor and the plasmonic metal are in contact, the hot electrons can be injected into the conduction band of the semiconductor, promoting the charge transfer process, since they have enough energy to overcome the Schottky barrier. Near field effect takes place when the metal NPs are not in contact with semiconductor and hence the process of electron-hole pairs formation can be induced by high intensity electric field, in close proximity to noble metal NPs [21].

Under the investigated experimental conditions, the "hot electrons" generation can be assumed as possible mechanism to account for the experimental evidences. Indeed, the synthesis of TiO_2/AuNRs was designed in order to enable the direct growth of TiO_2 domains on AuNRs substrates, without any intermediate dielectric layer. Such a condition allows the generation of "hot electrons" from the plasmonic NPs and the subsequent electron transfer from the metal to the semiconductor. It was recently demonstrated that the generation of hot electrons under visible light irradiation is more efficient for anisotropic NPs like Au NRs respect to Au nanospheres [14]. In the TiO_2/AuNRs 450 °C the employed calcination temperature allowed to preserve the anisotropy of Au domains, thus explaining its higher photocatalytic activity, under visible light irradiation, respect to the TiO_2/AuNRs calcinated at 650°, that is a temperature value able to induce a reshaping of the Au domains, finally leading to spheroidal Au NPs. Conversely to the spherical Au NPs in the of TiO_2/AuNRs sample obtained at 650 °C, the anisotropy of AuNRs in the sample calcinated at 450 °C can result much more effective for the exploitation of the NIR fraction of visible light, in order to promote the "hot electron" generation. Notably, the comparison between the kinetic constants of TiO_2/AuNRs 450 °C and TiO_2/AuNRs 250 °C calculated for the NA photodegradation reactions, suggests that the anisotropy is not the only parameter responsible for the improved photocatalytic activity of TiO_2/AuNRs 450 °C. Indeed, in the TiO_2/AuNRs 450 °C the synthesis conditions can promote an improved surface interaction between TiO_2 and AuNRs with a consequent increased production of Reactive Oxygen Species (ROS) upon the "hot electron" injection in the TiO_2 CB.

4. Conclusions

The preparation, characterization and investigation of the photocatalytic properties of a novel nanocomposite photocatalyst based on TiO_2 and Au NRs is described and its impact on photocatalytic degradation under UV and visible light of two organic compounds was demonstrated.

AuNRs modified TiO_2 nanocomposites were prepared on the scale up to tens of grams by a general co-precipitation method and the calcination temperature was investigated in order to elucidate the role of such a parameter on the photocatalytic performance of the plasmonic photocatalyst. The comprehensive characterization carried out by XRD, TEM, SEM and DR spectroscopy, shows that the Au NRs in TiO_2/AuNRs nanocomposite mainly retained their shape and the size up to 450 °C, while at higher calcination temperatures a reshaping of the Au NPs was observed, resulting into the conversion of the NRs into spheroidal structures. The incorporation of AuNRs in TiO_2 NPs aggregates has been found to provide protection against shape reshuffling up to 450 °C.

The photocatalytic activity of the TiO_2/AuNRs nanocomposite evaluated by performing degradation of the two different target compound, MB and NA demonstrated that the best performing catalyst is obtained when the prepared nanocomposite is calcined at 450 °C, being able to effectively catalyse MB and NA under UV light and visible light,

respectively, 2.5 and 3.2 times higher than the commercially available TiO_2P25 Evonik used as a reference material. In addition, the reaction catalysed by TiO_2/AuNRs nanocomposite calcined at 450 °C was up to 13 times faster than that catalysed by bare TiO_2-based catalysts for the two target compounds.

The photocatalytic performances have been discussed on the basis of the morphological and structural features of the investigated nanocomposites, calcined at the different temperature values, and the role of the plasmonic domain has been demonstrated responsible of the enhanced photocatalytic activity of the proposed nanocomposite materials.

The TiO_2/AuNRs nanocomposite demonstrated to be an innovative material with high photocatalytic performance, providing a new platform for applications in photocatalysis under visible light, a great promise for the degradation of organic molecules, including relevant pharmaceutical products. The technological viability of the proposed plasmonic nanocomposite is further strengthen by the simple and promptly up-scalable synthetic procedure used for its preparation.

Appendix A. Supplementary data

Supplementary material related to this article can be found, in the online version, at doi:https://doi.org/10.1016/j.apcatb.2018.11.002.

References

[1] H. Wang, L. Zhang, Z. Chen, J. Hu, S. Li, Z. Wang, J. Liu, X. Wang, Semiconductor heterojunction photocatalysts: design, construction, and photocatalytic performances, Chem. Soc. Rev. 43 (2014) 5234–5244.

[2] Y. Ben-Shahar, U. Banin, Hybrid semiconductor–metal nanorods as photocatalysts, Top. Curr. Chem. 374 (2016) 54.

[3] S.T. Kochuveedu, Y.H. Jang, D.H. Kim, A study on the mechanism for the interaction of light with noble metal-metal oxide semiconductor nanostructures for various photophysical applications, Chem. Soc. Rev. 42 (2013) 8467–8493.

[4] M. Pelaez, N.T. Nolan, S.C. Pillai, M.K. Seery, P. Falaras, A.G. Kontos, P.S.M. Dunlop, J.W.J. Hamilton, J.A. Byrne, K. O'Shea, M.H. Entezari, D.D. Dionysiou, A review on the visible light active titanium dioxide photocatalysts for environmental applications, Appl. Catal. B 125 (2012) 331–349.

[5] A. Truppi, F. Petronella, T. Placido, M. Striccoli, A. Agostiano, M. Curri, R. Comparelli, Visible-light-active TiO2-based hybrid nanocatalysts for environmental applications, Catalysts 7 (2017) 100.

[6] Z. Xuming, C. Yu Lim, L. Ru-Shi, T. Din Ping, Plasmonic photocatalysis, Rep. Prog. Phys. 76 (2013) 046401.

[7] V. Subramanian, E.E. Wolf, P.V. Kamat, Catalysis with TiO2/gold nanocomposites. Effect of metal particle size on the fermi level equilibration, J. Am. Chem. Soc. 126 (2004) 4943–4950.

[8] A. Bumajdad, M. Madkour, Understanding the superior photocatalytic activity of noble metals modified titania under UV and visible light irradiation, Phys. Chem. Chem. Phys. 16 (2014) 7146–7158.

[9] U. Banin, Y. Ben-Shahar, K. Vinokurov, Hybrid semiconductor–metal nanoparticles: from architecture to function, Chem. Mater. 26 (2014) 97–110.

[10] T.A. El-Brolossy, T. Abdallah, M.B. Mohamed, S. Abdallah, K. Easawi, S. Negm, H. Talaat, Shape and size dependence of the surface plasmon resonance of gold nanoparticles studied by photoacoustic technique, Eur. Phys. J. Spec. Top. 153 (2008) 361–364.

[11] L. Liu, S. Ouyang, J. Ye, Gold-nanorod-photosensitized titanium dioxide with wide-range visible-light harvesting based on localized surface plasmon resonance, Angew. Chem. Int. Ed. 52 (2013) 6689–6693.

[12] L. De Sio, G. Caracciolo, F. Annesi, T. Placido, D. Pozzi, R. Comparelli, A. Pane, M.L. Curri, A. Agostiano, R. Bartolino, Photo-thermal effects in gold nanorods/DNA complexes, Micro Nano Syst. Lett. 3 (2015) 1–9.

[13] R. Comparelli, T. Placido, N. Depalo, E. Fanizza, M. Striccoli, M.L. Curri, Synthesis and Surface Engineering of Plasmonic Nanoparticles, Active Plasmonic Nanomaterials, Pan Stanford, 2015, pp. 33–100.

[14] A. Sousa-Castillo, M. Comesaña-Hermo, B. Rodríguez-González, M. Pérez-Lorenzo, Z. Wang, X.-T. Kong, A.O. Govorov, M.A. Correa-Duarte, Boosting hot electron-driven photocatalysis through anisotropic plasmonic nanoparticles with hot spots in Au–TiO2 nanoarchitectures, J. Phys. Chem. C 120 (2016) 11690–11699.

[15] T. Placido, R. Comparelli, F. Giannici, P.D. Cozzoli, G. Capitani, M. Striccoli, A. Agostiano, M.L. Curri, Photochemical synthesis of water-soluble gold nanorods: the role of silver in assisting anisotropic growth, Chem. Mater. 21 (2009) 4192–4202.

[16] A. Altomare, M.C. Burla, C. Giacovazzo, A. Guagliardi, A.G.G. Moliterni, G. Polidori, R. Rizzi, Quanto: a rietveld program for quantitative phase analysis of polycrystalline mixtures, J. Appl. Crystallogr. 34 (2001) 392–397.

[17] A. Mills, An overview of the methylene blue ISO test for assessing the activities of photocatalytic films, Appl. Catal. B 128 (2012) 144–149.

[18] L. Ge, J. Chen, X. Wei, S. Zhang, X. Qiao, X. Cai, Q. Xie, Aquatic photochemistry of fluoroquinolone antibiotics: kinetics, pathways, and multivariate effects of main water constituents, Environ. Sci. Technol. 44 (2010) 2400–2405.

[19] F. Petronella, S. Diomede, E. Fanizza, G. Mascolo, T. Sibillano, A. Agostiano, M.L. Curri, R. Comparelli, Photodegradation of nalidixic acid assisted by TiO2 nanorods/Ag nanoparticles based catalyst, Chemosphere 91 (2013) 941–947.

[20] P.V. Kamat, Photophysical, photochemical and photocatalytic aspects of metal nanoparticles, J. Phys. Chem. B 106 (2002) 7729–7744.

[21] F. Petronella, A. Truppi, T. Sibillano, C. Giannini, M. Striccoli, R. Comparelli, M.L. Curri, Multifunctional TiO2/FexOy/Ag based nanocrystalline heterostructures for photocatalytic degradation of a recalcitrant pollutant, Catal. Today 284 (2017) 100–106.

[22] R. Ancora, M. Borsa, L. Cassar, Titanium Dioxide Based Photocatalytic Composites and Derived Products on a Metakaolin Support, Italcementi S.P.A., Italy, 2009.

[23] R. Comparelli, E. Fanizza, M. Striccoli, M.L. Curri, Characterization of in-organicnanostructuredmaterials by electron microscopy, in: A. Dibenedetto, M. Aresta (Eds.), Inorganic Micro-and Nanomaterials: Synthesis and Characterization, Walter de Gruyter, 2013.

[24] M. Casavola, R. Buonsanti, G. Caputo, P.D. Cozzoli, Colloidal strategies for preparing oxide-based hybrid nanocrystals, Eur. J. Inorg. Chem. 2008 (2008) 837–854.

[25] P. Nbelayim, G. Kawamura, W. Kian Tan, H. Muto, A. Matsuda, Systematic characterization of the effect of Ag@TiO2 nanoparticles on the performance of plasmonic dye-sensitized solar cells, Sci. Rep. 7 (2017) 15690.

[26] P. Górska, A. Zaleska, E. Kowalska, T. Klimczuk, J.W. Sobczak, E. Skwarek, W. Janusz, J. Hupka, TiO2 photoactivity in vis and UV light: the influence of calcination temperature and surface properties, Appl. Catal. B 84 (2008) 440–447.

[27] J.-G. Yu, H.-G. Yu, B. Cheng, X.-J. Zhao, J.C. Yu, W.-K. Ho, The effect of calcination temperature on the surface microstructure and photocatalytic activity of TiO2 thin films prepared by liquid phase deposition, J. Phys. Chem. B 107 (2003) 13871–13879.

[28] A. Cybula, J.B. Priebe, M.-M. Pohl, J.W. Sobczak, M. Schneider, A. Zielińska-Jurek, A. Brückner, A. Zaleska, The effect of calcination temperature on structure and photocatalytic properties of Au/Pd nanoparticles supported on TiO2, Appl. Catal. B 152–153 (2014) 202–211.

[29] https://www.aerosil.com/product/aerosil/en/effects/photocatalyst/Pages/default.aspx.

[30] Q. Yang, C. Xie, Z. Xu, Z. Gao, Y. Du, Synthesis of highly active sulfate-promoted rutile titania nanoparticles with a response to visible light, J. Phys. Chem. B 109 (2005) 5554–5560.

[31] J. Gardy, A. Hassanpour, X. Lai, M.H. Ahmed, Synthesis of Ti(SO4)O solid acid nano-catalyst and its application for biodiesel production from used cooking oil, Appl. Catal. A Gen. 527 (2016) 81–95.

[32] R.M. de Almeida, L.K. Noda, N.S. Gonçalves, S.M.P. Meneghetti, M.R. Meneghetti, Transesterification reaction of vegetable oils, using superacid sulfated TiO2–base catalysts, Appl. Catal. A Gen. 347 (2008) 100–105.

[33] M.E. Birch, T.A. Ruda-Eberenz, M. Chai, R. Andrews, R.L. Hatfield, Properties that influence the specific surface areas of carbon nanotubes and nanofibers, Ann. Occup. Hyg. 57 (2013) 1148–1166.

[34] F. Petronella, M.L. Curri, M. Striccoli, E. Fanizza, C. Mateo-Mateo, R.A. Alvarez-Puebla, T. Sibillano, C. Giannini, M.A. Correa-Duarte, R. Comparelli, Direct growth of shape controlled TiO2 nanocrystals onto SWCNTs for highly active photocatalytic materials in the visible, Appl. Catal. B 178 (2015) 91–99.

[35] I. Ros, T. Placido, V. Amendola, C. Marinzi, N. Manfredi, R. Comparelli, M. Striccoli, A. Agostiano, A. Abbotto, D. Pedron, R. Pilot, R. Bozio, SERS properties of gold nanorods at resonance with molecular, transverse, and longitudinal plasmon excitations, Plasmonics (2014) 1–13.